Nanoscale

Accepted Manuscript

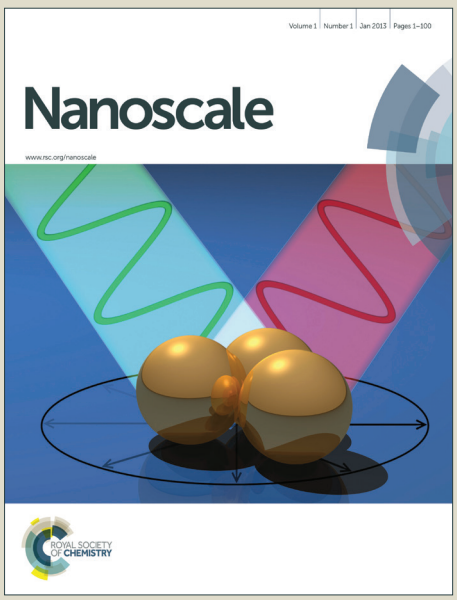

ROYAL SOCIETY OF CHEMISTRY

www.rsc.org/nanoscale

Fragmentation and exfoliation of low-dimensional materials; a statistical approach.

Konstantinos Kouroupis-Agalou[1], Andrea Liscio[1], Emanuele Treossi,[1,2] Luca Ortolani[3], Vittorio Morandi[3], Nicola Maria Pugno[4], Vincenzo Palermo[1,2]*

[1] Istituto per la Sintesi Organica e la Fotoreattività-Consiglio Nazionale delle Ricerche (ISOF-CNR), via Gobetti 101, 40129 Bologna, Italy.

[2]Laboratorio MIST.E-R Bologna, via Gobetti 101, 40129 Bologna (Italy)

[3] Istituto per la Microelettronica e Microsistemi-Consiglio Nazionale delle Ricerche (IMM-CNR), via Gobetti 101, 40129 Bologna, Italy.

[4] Dipartimento di Ingegneria Civile, Ambientale e Meccanica, Università di Trento, via Mesiano, 77 I-38123 Trento (Italia)

E-mail: palermo@isof.cnr.it

Abstract

A main advantage for applications of Graphene and related 2-dimensional materials is that they can be produced on large scales by liquid phase exfoliation. The exfoliation process shall be considered as a particular fragmentation process, where the 2-dimensional (2D) character of the exfoliated objects will influence significantly fragmentation dynamics as compared to standard materials. Here, we used automatized image processing of Atomic Force Microscopy (AFM) data to measure, one by one, the exact shape and size of thousands of nanosheets obtained by exfoliation of an important 2D-material, Boron Nitride, and used different statistical functions to model the asymmetric distribution of nanosheets sizes typically obtained. Being the resolution of AFM much larger than the average sheet size, analysis could be performed directly at the nanoscale, and at single sheet level. We find that the size distribution of the sheets at a given time follows a Log-normal distribution, indicating that the exfoliation process has a "typical" scale length that changes with time and that exfoliation proceeds through the formation of a distribution of random cracks that follow Poisson statistics. The common validity of this model implies that size distribution does not depend on the different preparation methods used, but is a common feature in the exfoliation of this material.

The huge scientific and technological interest for graphene has triggered in last years the development of a wide range of techniques to produce and process nanosheets that, having nanometric thickness and mesoscopic lateral size, shall be considered as *quasi* 2-dimensional (2D) objects. Besides their novel properties, even the way these 2D sheets are produced in solution, by exfoliation, [1] is an original process, still not completely understood.

The exfoliation of a 2D object from a 3D bulk material is a process spanning from nano- to meso-scale due to bubble cavitation, intercalation and disruptive fragmentation, as we described in recent work.[2] Exfoliation always yields a poly-dispersed range of nanosheets thickness and lateral size. When characterizing these 2D sheets solutions, their average size and size standard deviation are commonly reported, in this way assuming that their size follows a "Gaussian" (a.k.a. "normal") distribution. Conversely, the experimental data show that the size distribution of these materials is highly asymmetric and non-Gaussian.

Noteworthy, this asymmetry in size distribution shall be observed in very different systems such, as example, the distribution of chemical elements in rocks, the species abundance in biology, the lengths of latent periods of infectious diseases in medicine, the distribution of galaxies in astronomy (Fig. 1).[3,4]

A better modelling of the size distribution of 2D materials is needed both from a fundamental point of view (to understand the exfoliation mechanism) and a technological point of view (to improve the metrology of 2D materials for applications and quality control).

Here, we used image processing of Atomic force Microscopy (AFM) images to study the exfoliation and fragmentation process of a well-known 2D material, Boron Nitride (BN, Fig. 2) exfoliated in solution with two technologically relevant techniques: ultrasonication and ball milling. Exfoliated BN nanosheets are deposited on silicon and their size distribution is measured

by AFM and an image analysis software, performing in this way statistics on *all* the sheets present on the surfaces, for a total of >6000 sheets, as compared to the tens of sheets analysed by manual TEM statistics typically used for this task.[5] Being the resolution of AFM much larger than the average sheet size, the exact shape of each sheet shall be included in the statistics, allowing to cross-relate the length, the area and length/width ratio of each sheet in each sample.[6]

By using a large statistical population we are confident to discriminate the most suitable analytic function able to reproduce the achieved fragment size distribution. As example, studying the galaxy distribution Brown *et al*. demonstrated that the universe underwent a single fragmentation event, separating into protogalactic volumes at a relatively early stage after the Big Bang.[7]

As test material, we chose not to use the well-known graphene but used Boron Nitride, a relatively less studied 2D material which has anyhow huge scientific and industrial interest, because it can be used as a monoatomic insulating layer for graphene-based electronic devices,[8, 9] or as a bulk additive in polymers.[10]

Fig. 2 shows Scanning Electron Microscopy (SEM) images of typical BN flakes, and solutions obtained from such flakes by sonication or ball milling in isopropyl alcohol (IPA). The solutions obtained are stable for more than 6 months. BN solutions show a whitish colour and a strong light scattering (Fig. 2b), due to the presence of the BN nanosheets. Details of the different exfoliation procedures used are reported in the supporting information (SI). After exfoliation, the nanosheets were spin coated on silicon and measured by AFM (Fig. 2c,d).

To quantify the sheet size obtained with different techniques, we used an image analysis software able to detect automatically individual sheets and measure their area and lateral size

(Fig. 2e).[11] While AFM can easily give high-resolution images of the flakes and allow manual measurements of their size, several steps (image flattening, threshold selection, etc.) and careful analysis are required to obtain quantitative results, as detailed in SI.

By using this approach, we could detect and digitalize hundreds of flakes having thickness down to 1 nm, deposited on areas of 1 - 400 μm^2.

Definition of sheet size

A particular issue in characterizing 2D nanosheets is to define the "size" of the sheets, because they have highly irregular shapes; we shall define for each sheet a given length *L*, measured along the main axis, and a width *W* measured perpendicular to it (Fig. 2d).

For perfectly rectangular sheets the area *A* would be simply $L \cdot W$. This is not true for irregular shapes such as the ones typically obtained by exfoliation of 2D materials. However, the image analysis software allows to measure pixel by pixel the area of each sheet, and use this as the relevant parameter to monitor exfoliation.

To have a reliable parameter, not depending on a particular shape, we thus used as relevant "size" of the sheets the square root of the sheet area, measured pixel by pixel: $s = \sqrt{Area_{meas}}$. In case of perfectly rectangular shapes, this would be simply $s = \sqrt{L \cdot W}$; for irregular sheets, this has the same dimensionality but is a more reliable parameter than length *L*. Differently from *L*, *s* does not depend on sheet shape, but only on the exact area.

Modelling of fragmentation processes

Fig. 3 shows that the statistical distributions of sheet sizes obtained with either sonication or ball milling do not follow a Gaussian (a.k.a. "normal") distribution, but are strongly asymmetric

and positively skewed, with a tail due to the presence of larger sheets in all samples. All the physical dimensions of the exfoliated sheets (length, width, area, thickness) show the same asymmetric, non-Gaussian distribution (some examples are shown in fig. S1 in SI).

In general, skewed functions are the most general case to describe the asymmetric distribution of a physical observable (e.g., the size particle in powders or polymer blends). As example, one of the most used distribution is the Poisson one, a discrete distribution that estimates the probability of a given number of events occurring in a fixed interval of space (distance, area or volume) and/or time if these events occur with a known average rate and independently from each other.[12] Poisson distribution is asymmetric and represents a very general case containing the well know and commonly used Gaussian distribution which is obtained as a limit of the Poisson one in the case of the total number of events $N \rightarrow \infty$.

The Gaussian is a continuous symmetric distribution with the domain defined at all $\Re$; in particular the position of the peak (mode) coincides with the mean value (μ) and the median and the peak width are directly correlated with the standard deviation (σ); for these reasons, the Gaussian function is widespread and is commonly used to model several kinds of real distributions.

Given a distribution $f(\mu,\sigma)$, where μ is the distribution average and σ the distribution standard deviation, the Gaussian is a good approximation for $\mu/\sigma >> 1$. This condition is not satisfied for the measured length, width and size distribution of the BN sheets, as clearly shown in Fig. 1,3 and Fig. S1. Moreover, the studied observables cannot be negative and the Gaussian distributions cannot be used to reproduce the measured ones.

For exfoliated 2D nanosheets the mean value will not correspond to the median or to the highest peak of the size distribution, and the standard deviation will not be proportional to the half width of the distribution peak.

On the mathematic side, the importance of the Gaussian function is due to its role in the Central Limit Theorem, which loosely says that the *sum* of a large number of independent quantities tends to have a Gaussian form, independent of the probability distribution of the individual measurements. This is the case, as example, of the distribution of the *x,y,z* coordinates of particles diffusing in a solvent, coming from the sum of random scattering events.

When, instead, the final size is the result of the *product* of many independent, identically distributed actions, the final result is a highly skewed Log-normal distribution. The skewed shape obtained in all exfoliation processes can thus be explained as the result of a more general fragmentation process,[3] where the size s of a sheet changes at each "cutting" event i as $s_i = s_{i-1} / c$.

In order to find the most appropriate analytic function to model exfoliation, we compared three continuous probability distributions commonly used to study the fragmentation processes: (LN) Log-normal, (W) Weibull and (G) Gamma function. A comparison of the properties of these functions is reported in Table S1 in SI.

LN represents the distribution of a random variable whose logarithm is normally distributed. If the random variable x is Log-normally distributed, then $X = \log(x)$ has a Gaussian distribution. LN is characteristic of a random multiplicative process, and has previously been used to describe many rock crushing processes.

Weibull function was the first function applied by Rosin & Rammler in 1933 to describe a particle size distribution.[13] W function describes the size distribution given by a series of

fragmentation events which are not constant and whose rate is proportional to a power of size: $\tau = s^k$, where k is the exponent of the power law.

Gamma Function is the generalization of the Maxwell-Boltzmann distribution and it is used to study the collisional fragmentation problem.[14] Moreover, G distribution functions are known to provide a very good fit to the distribution of cell sizes in Voronoi textures (i.e area in 2D partitioned Euclidean spaces).[15]

Fig. 3 shows the measured size distribution of sheet size *f(s)*, obtained by sonication and ball milling with high and low power (see SI for details). To avoid any artefacts we used for the fit only sheets having *s>50* nm, significantly larger than AFM resolution. Experimental data have been fitted using different statistical distributions: LN (black line), W (blue line) and G (green line). In general, it is difficult to discriminate between the Log-normal, Weibull and even Gamma distributions in particle size distribution curves as evident from the figure; the coefficient of determination (R^2) is 0.93 – 0.94 for all the three curves (the closer is R^2 value to 1, the better is the fitting).

In order to overcome this well-known problem (see[16] as example), we studied the complementary cumulative distribution functions: $N(s) = N(s_{TOT}) - \int_0^s f(x)dx$, calculated by the best fits of three curves. Given a size *s*, *N(s)* function indicates the number of sheets *larger* than *s*, for this reason it's also called *survival* or *reliability* function.

The measured distribution and the calculated curves are displayed in Fig. 4 using a semi-log scale visualization. The comparison between all the curves shows clearly that the experimental distribution *N(s)* of sheet sizes follows a Log-normal curve. Sheet distribution obtained with very different methods (sonication and ball milling) can thus be fitted using the same model, suggesting that the sheet size distribution does not depend on the details of the preparation

methods, but is instead a common feature in the exfoliation of 2D materials. This kind of "universal behaviour" is not surprising, and has been observed in different disciplines.[3] The presence of Log-normal behaviour is characteristic of a random multiplicative process; it indicates that exfoliation follows a linear fragmentation model, i.e. a process where the fragmentation is only driven by external source (in this case, ultrasounds or milling balls) and where the repeated collisions between fragments can be neglected. [17]According to Kolmogorov theory[18] the LN distribution represents the final size distribution in the limit of small BN fragments originated by a "mother cluster" which broke into random-sized fragments through a stochastically determined process (Markov process). The regime of limit of small fragments corresponds to the case in which the fragmentation is completely described by rupture-like breakup events while the erosion-like events (described by a size distribution with bimodal shape) can be completely neglected.

Not only many different variables distributions follow a Log-normal behaviour, but even the width of these Log-normal distributions (calculated as the variance of the normalized unit $S = \ln s / s_{mode}$) range from about 0.2 to 0.5 in several different cases in literature.[19]

We calculated the effective distribution widths V_{Eff} for all our samples (fig. 5); while, as could be expected, variance increases slightly with processing time, all values found lay within the range 0.2-0.5 indicating that the fragmentation event is nearly binary, i.e., one flakes is divided in two flakes, with no "multiple fragmentation" events.[19] In simpler words, in the assumed fragmentation $s_i = s_{i-1} / c$ we have $c \approx 2$.

Last but not least, it can be seen that the distribution decay is linear for large s, indicating that the exfoliation proceeds through the formation of a distribution of random cracks that follows Poisson statistics.[7, 20]

Shape analysis of the exfoliated sheets

Using image processing of the AFM images, we could also calculate the length/width aspect ratio for all the samples. We found that, even if the sheet's size spans over nearly two orders of magnitude (within the range between 30 and 1000 nm), the overall length/width (*L*/*W*) ratio is fairly constant, being ≈*2.8* for sonication and ≈*2.6* for milling (see Fig. 6a; all graphs showing the data points analysed are shown in Fig. S2). Summarizing, (*L*/*W*) ratio only depends on the fragmentation technique, but doesn't show any appreciable variation on the processing time and/or processing conditions.

To check if this ratio is simply due to a random distribution of sheets' shape, we compared it with the *L*/*W* ratio of artificial, computer-generated rectangles having random sides *a* and *b* spanning the same size range observed for real nanosheets. Fig. 6 shows length vs. width plots obtained from experimental data (Fig. 6a) or from computer-generated rectangles with random, uncorrelated length and width (Fig. 6b).

The experimental data in Fig. 6a were obtained from the AFM analysis of more than 1400 sheets produced by sonication and ball milling at different times. The artificial data in Fig. 6b were instead obtained generating rectangles were the sides of each rectangle are uncorrelated, even if having a Log-normal distribution with the same mean values and standard deviation of the experimental ones.

The calculated distribution in Fig. 6b clearly shows different behaviour respect to the measured ones and has a *L*/*W* ratio = 4.0±0.1, significantly larger than that obtained from the measurements. The experimental length and width of sheets are thus correlated, as visible in Fig. 6a and Fig. S2, and their ratio is not a random value. This suggests that the shear stress of 2D sheets along different directions yields fracture probability of sheets having a preferred *L*/*W*

aspect ratio. This ratio is slightly larger for sonication (*L/W≈2.8*, likely due to the aligning effect of collapsing cavitation bubbles[21]) than in ball milling, (*L/W≈2.6)*, where shear force can cleave the BN flakes from their outer surfaces, while the compression force can crush and delaminate thin nanoplatelets acting on their edge.[22] Scanning Electron microscopy (SEM) images of BN mesoscopic flakes cleaved by different shear forces are shown in Fig. 7. The effects of shear and compression action of the milling spheres is visible on several flakes, with BN stacks shifted over each other, showing folds not only on the surface of the platelets, due to the shear force of balls rolling over the top surface of the particle, but also *inside* the platelets due to the compression force of milling balls colliding with the edge of the particles.[23]

Sheet size evolution with time

We studied the evolution of average size at increasing processing times, that we call $s_{mean}(t)$. As mentioned above, we should keep in mind that this average value will not correspond to the median or to the highest peak of the size distribution *N(s)*, because it is not Gaussian.

The AFM size analysis, performed on surfaces at the nanoscale, gives similar results to macroscopic DLS measurements performed in solution, but with an offset (DLS gives an estimated size that is larger than the AFM measured one of ca. 20%, see SI for more details).

LN distribution is observed for all the used fragmentation procedures and for different times. Hansen et al.[24] observed that the size scales with time as an inverse power-law: $s_{mean} \propto t^{-1/\lambda}$ (Fig. S3) where λ (a.k.a. homogeneity index) is the exponent of the overall rate of breakup $a(s) \propto s^{\lambda}$. According to this model, higher values of λ indicate that fragmentation speed is strongly dependent on sheet size.

In our sonication experiments, the value of λ (homogeneity index) goes from 8±1 to 4.5±0.6 by increasing sonication power, suggesting that in high power sonication, with high shear rates, the probability of breaking is more uniform for sheets of different sizes.

A similar inverse power-law dependence (with $\lambda=2$) as been recently reported by Khan et al.[25] exploiting a theory previously involved to reproduce the length distributions of sonication of 1D nanotubes[21] to model the size reduction of sonicated graphene sheets.

We note that the application of models developed for 1D objects to 2D shapes is not straightforward. A 1D nanotube can be defined with a single dimension *L* and can broken in just one direction, perpendicular to its long axis; conversely, a 2D sheet can be broken in different directions, shall have different length/width ratio, and thus have a different evolution of the average area or average lateral size with processing time. Moreover, the power law should depend on the power dissipated during the fragmentation events.

Finally, the statistical procedure described here was used to compare the average size of BN sheets obtained by high sonication and milling. The asymptotic values are 105±7 nm and 100±8 nm, for high and low power sonication, while for milling we obtain 142±8 nm and 136±4 nm, respectively for high and low power. We underline that (differently from size distributions discussed above) these numbers are not universal results but depend on the exfoliation conditions used such as processing conditions, time, solvent, etc.

To test the processability of the obtained materials, we used them to produce BN paper membranes by filtering the solution on filter paper. Upon removal of the filter, we obtained uniform membranes of BN, robust enough to be handled and further processed (Fig. S5).

In conclusion, we characterized the size distribution of BN nanosheets produced in solution by sonication and ball milling. In all the different samples tested, the cumulative size distribution of the sheets at a given time follows a Log-normal distribution.

We did not observe a power-law distribution of sizes that would imply a scale-invariant exfoliation process. The failure of the power-law curve indicates that the exfoliation process does not follow fractal law, but rather has a "typical" sheet scale length.

The Log-normal best-fit curves obtained show a very good linearity in semi-log scale (black lines in Fig. 4) within the data range ($R^2 = 0.9936$) This behaviour corresponds to the simplest case of the empirical Rosin-Rammler equation,[26] indicating that for both sonication and ball-milling techniques, exfoliation proceeds through the formation of a distribution of random cracks that follow Poisson statistics.[7, 20] The fragmentation can be simply described as process mainly driven by external source and completely described by rupture-like breakup events.

Acknowledgements

The research leading to these results has received funding from the European Union Seventh Framework Programme under grant agreement n°604391 Graphene Flagship, the EC Marie-Curie ITN-GENIUS (PITN-GA-2010-264694), the FET project UPGRADE (project no. 309056), the Operative Program FESR 2007-2013 of Regione Emilia-Romagna – Attività I.1.1 and the European Research Council (ERC StG 2011 BIHSNAM on "Bio-inspired hierarchical super-nanomaterials").

Supporting Information Available: Exfoliation methods, Image analysis procedure, Comparison of sheet size on surfaces and in solution.. This material is available free of charge via the Internet.

FIGURES

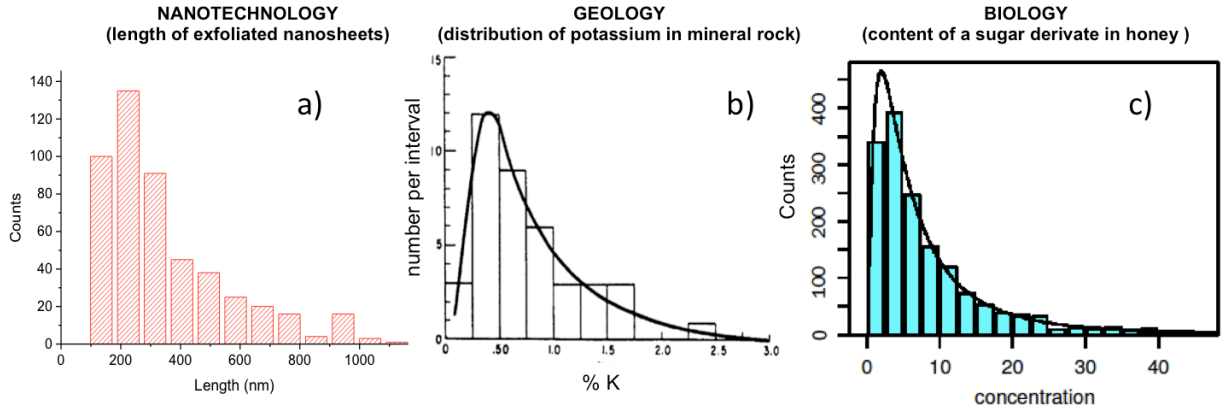

Fig. 1 Comparison of the typical size distribution obtained by exfoliation with other distributions observed in 2D materials, geology and biology. a) Histogram of length distribution of BN nanosheets length obtained by liquid phase exfoliation. b) Distribution of potassium in mineral rock.[4] c) content of hydroxymethylfurfurol in honey.[3]

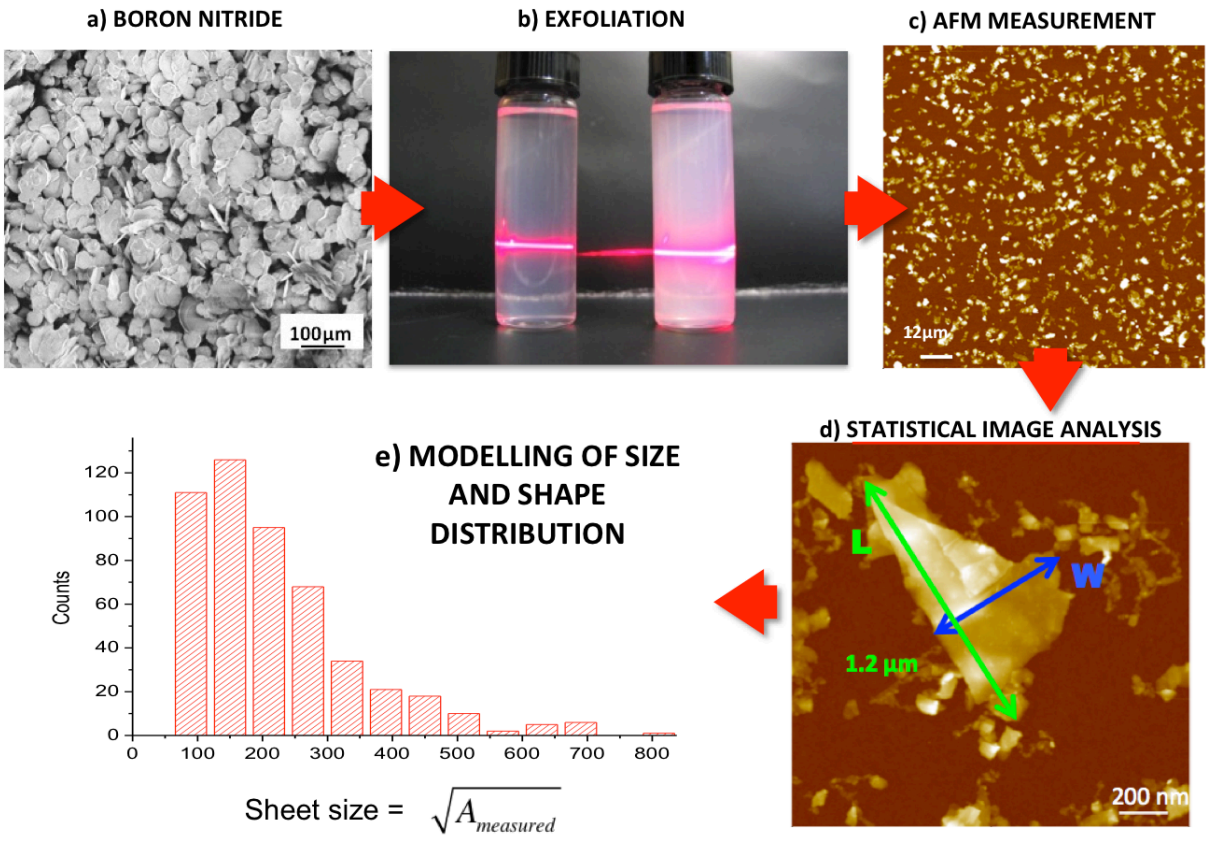

Fig. 2 a) SEM image of the pristine BN flakes used for exfoliation. b) Exfoliated solutions of BN in isoproanol, showing strong scattering due to the dispersed flakes. c) AFM image of BN nanosheets spin coated on silicon oxide substrates. d) Zoom-in of a single nanosheet, showing the typical, non exact way to estimate of its length and width. e) Histogram distribution of sheet size obtained instead measuring precisely the area of each sheet.

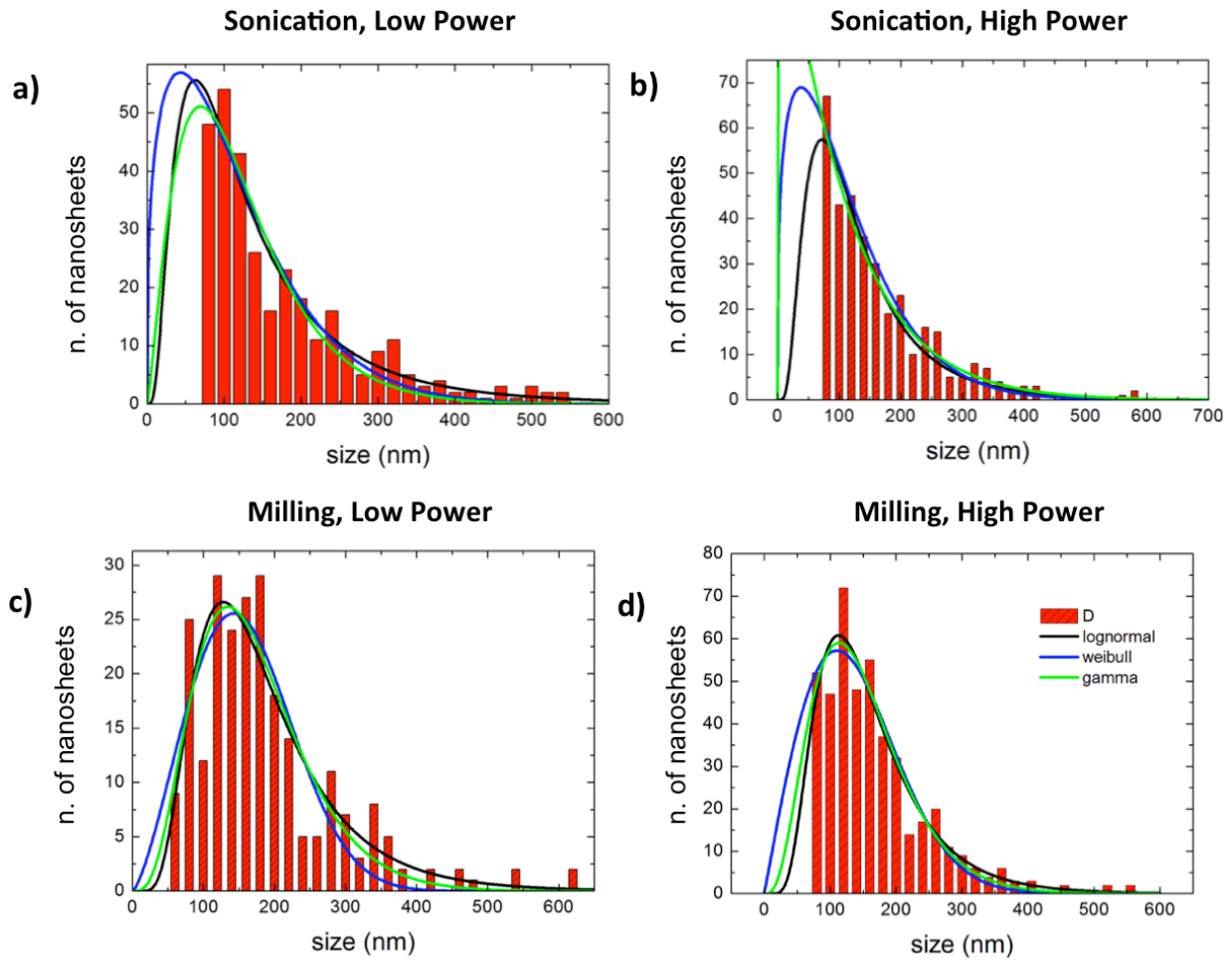

Fig. 3 Nanosheet size distribution obtained with sonication and ball milling, using different preparation conditions. A fit of the experimental data using Log-normal, Weibull or Gamma distributions is also reported in black, blue, green lines respectively.

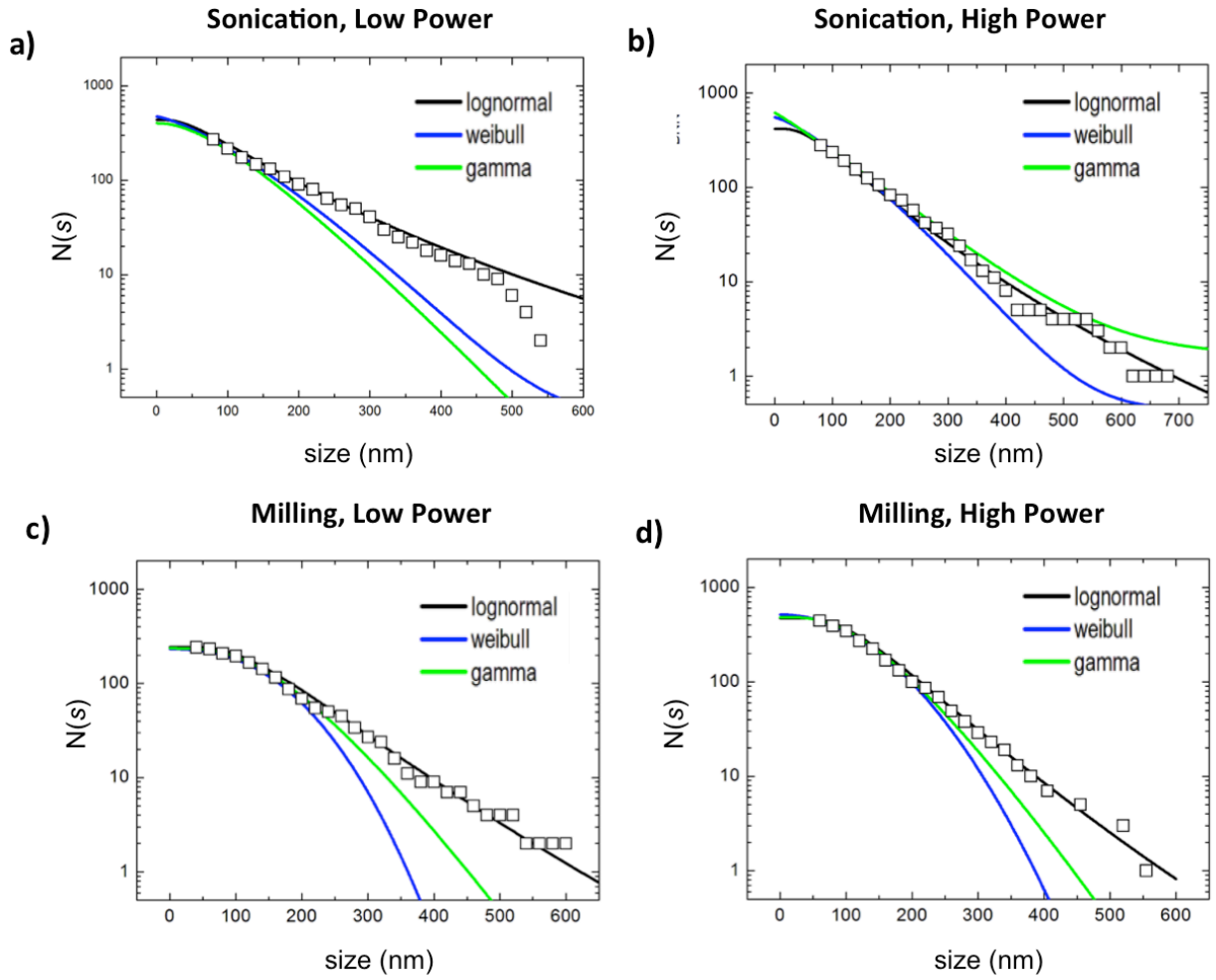

Fig. 4 Survival distribution functions (empty squares) corresponding to the data shown in fig. 3. A fit of the experimental data using Log-normal, Weibull or Gamma distributions is also reported in black, blue, green lines respectively.

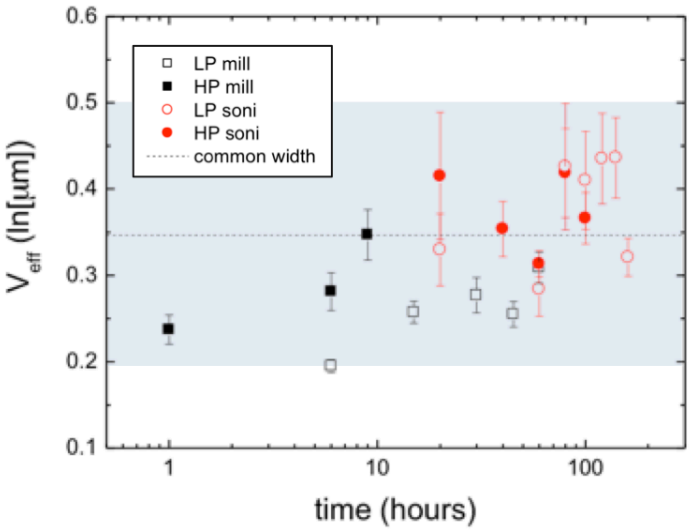

Fig. 5 Effective variance of the Log-normal distribution observed for all samples. The shaded area indicates the 0.2-0.5 "universal" variance observed in several different cases in literature.[19]

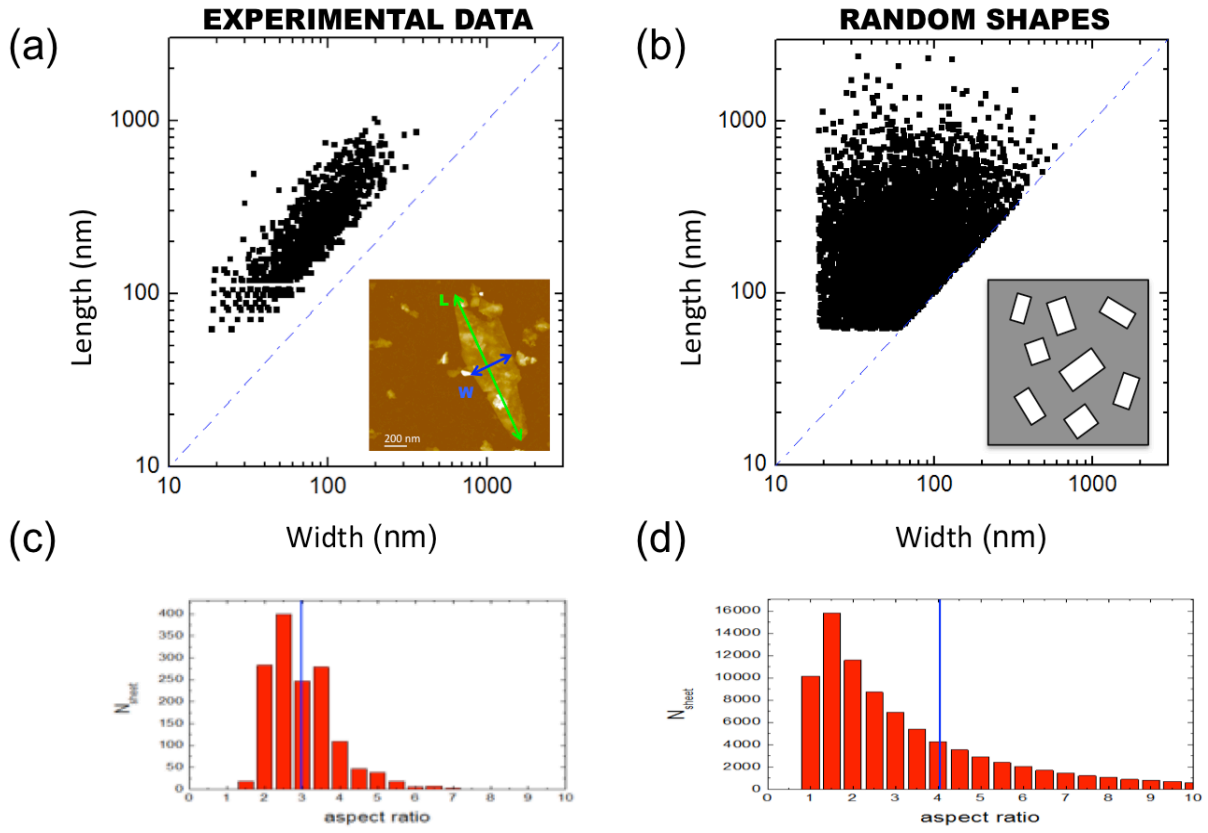

Fig. 6 Length/width plots of BN sheets (a) measured in the case of High power Sonication and (b) calculated by random distributions, plotted in Log-log scale. Blue dash-dot line represents the case of aspect ratio = 1. (c,d) Corresponding L/W ratio distributions (red bars) (c) measured in the case of High power Sonication and (d) calculated by random distributions. Blue vertical lines show the mean values.

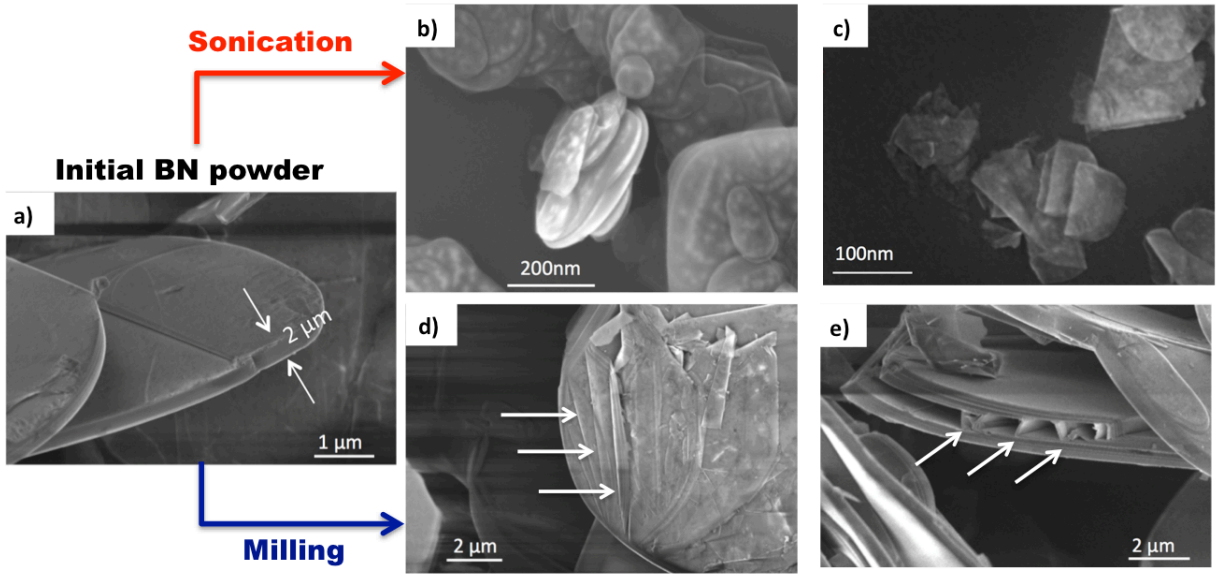

Fig. 7 SEM images showing the effect of different forces in BN exfoliation by milling and sonication

REFERENCES

1. J. N. Coleman, M. Lotya, A. O'Neill, S. D. Bergin, P. J. King, U. Khan, K. Young, A. Gaucher, S. De, R. J. Smith, I. V. Shvets, S. K. Arora, G. Stanton, H. Y. Kim, K. Lee, G. T. Kim, G. S. Duesberg, T. Hallam, J. J. Boland, J. J. Wang, J. F. Donegan, J. C. Grunlan, G. Moriarty, A. Shmeliov, R. J. Nicholls, J. M. Perkins, E. M. Grieveson, K. Theuwissen, D. W. McComb, P. D. Nellist and V. Nicolosi, *Science*, 2011, **331**, 568-571.
2. Z. Y. Xia, S. Pezzini, E. Treossi, G. Giambastiani, F. Corticelli, V. Morandi, A. Zanelli, V. Bellani and V. Palermo, *Advanced Functional Materials*, 2013, DOI: 10.1002/adfm.201203686.
3. E. Limpert, W. A. Stahel and M. Abbt, *Bioscience*, 2001, **51**, 341-352.
4. L. H. Ahrens, *Geochlmlca et Coemoehlmlca Acta*, 1957, **5**, 49-73.
5. Y. Hernandez, V. Nicolosi, M. Lotya, F. M. Blighe, Z. Y. Sun, S. De, I. T. McGovern, B. Holland, M. Byrne, Y. K. Gun'ko, J. J. Boland, P. Niraj, G. Duesberg, S. Krishnamurthy, R. Goodhue, J. Hutchison, V. Scardaci, A. C. Ferrari and J. N. Coleman, *Nature Nanotechnology*, 2008, **3**, 563-568.
6. J. Russier, E. Treossi, A. Scarsi, F. Perrozzi, H. Dumortier, L. Ottaviano, M. Meneghetti, V. Palermo and A. Bianco, *Nanoscale*, 2013, **5**, 11234-11247.
7. W. K. Brown, R. R. Karpp and D. E. Grady, *Astrophysics and Space Science*, 1983, **94**, 401-412.
8. L. Britnell, R. V. Gorbachev, R. Jalil, B. D. Belle, F. Schedin, A. Mishchenko, T. Georgiou, M. I. Katsnelson, L. Eaves, S. V. Morozov, N. M. R. Peres, J. Leist, A. K. Geim, K. S. Novoselov and L. A. Ponomarenko, *Science*, 2012, **335**, 947-950.
9. B. Hunt, J. D. Sanchez-Yamagishi, A. F. Young, M. Yankowitz, B. J. LeRoy, K. Watanabe, T. Taniguchi, P. Moon, M. Koshino, P. Jarillo-Herrero and R. C. Ashoori, *Science*, 2013, **340**, 1427-1430.
10. U. Khan, P. May, A. O'Neill, A. P. Bell, E. Boussac, A. Martin, J. Semple and J. N. Coleman, *Nanoscale*, 2013, **5**, 581-587.
11. , Editon edn., Scanning Probe Image Processor, version 2.0000, Image Metrology A/S, Lyngby, Denmark.
12. J. Frederick, *Statistical Methods In Experimental Physics (2Nd Edition)*, World Scientific Publishing Co Pte Ltd, Singapore, 2006.
13. P. Rosin and E. Rammler, *Institute of Fuel*, 1933, **7**, 29-36.
14. M. Kostoglou and A. J. Karabelas, *Journal of Colloid and Interface Science*, 2006, **303**, 419-429.
15. M. A. Fortes and P. N. Andrade, *Journal of Applied Physics*, 1988, **64**, 5157-5160.
16. G. M. Kondolf and A. Adhikari, *Journal of Sedimentary Research*, 2000, **70**, 456-460.
17. Z. Cheng and S. Redner, *Physical Review Letters*, 1988, **60**, 2450-2453.
18. N. A. Kolmogorov, *Transl. in English by Levin in NASA-TT F-12,287 (1969)*, 1941, **31**.
19. K. Hosoda, T. Matsuura, H. Suzuki and T. Yomo, *Physical Review E*, 2011, **83**.
20. D. L. Turcotte, *Journal of Geophysical Research-Solid Earth and Planets*, 1986, **91**, 1921-1926.
21. F. Hennrich, R. Krupke, K. Arnold, J. A. R. Stutz, S. Lebedkin, T. Koch, T. Schimmel and M. M. Kappes, *Journal of Physical Chemistry B*, 2007, **111**, 1932-1937.
22. Y. G. Yao, Z. Y. Lin, Z. Li, X. J. Song, K. S. Moon and C. P. Wong, *Journal of Materials Chemistry*, 2012, **22**, 13494-13499.

23. L. H. Li, Y. Chen, G. Behan, H. Z. Zhang, M. Petravic and A. M. Glushenkov, *Journal of Materials Chemistry*, 2011, **21**, 11862-11866.
24. S. Hansen, D. V. Khakhar and J. M. Ottino, *Chemical Engineering Science*, 1998, **53**, 1803-+.
25. U. Khan, H. Porwal, A. O'Neill, K. Nawaz, P. May and J. N. Coleman, *Langmuir*, 2011, **27**, 9077-9082.
26. J. J. Gilvarry, *Journal of Applied Physics*, 1961, **32**, 391.